Available online at www.sciencedirect.com
SCIENCE DIRECT
Journal of Sound and Vibration 293 (2006) 735–746
JOURNAL OF SOUND AND VIBRATION
www.elsevier.com/locate/jsvi

TGV disc brake squeal

X. Lorang[a], F. Foy-Margiocchi[b,*], Q.S. Nguyen[a], P.E. Gautier[b]

[a]*Laboratoire de Mécanique des Solides, Ecole polytechnique, 91128 Palaiseau, Cedex, France*
[b]*SNCF, Direction de l'Innovation et de la Technologie, 45 rue de londres, 75379 Paris, Cedex 08, France*

Accepted 26 August 2005
Available online 13 February 2006

Abstract

The discomfort generated by the noise emission of braking systems in trains has aroused recently many studies on the mechanical modelling of brake noise in France. A theoretical and numerical discussion on the phenomenon of brake squeal is given in this paper in relation with some experimental data. This study is based upon a flutter instability analysis giving unstable modes of the brake system under the contact and Coulomb friction.

1. Background

Brake squeal is a complex phenomenon which has been studied since the beginning of the 20th century. Lots of work has been motivated particularly by the automotive industry [1–3]. From a theoretical point of view, different types of model have been built in order to understand the generation of squeal [4] and to predict its frequencies. However, the prediction of squeal frequencies in real applications remains challenging.

In the initial prediction models, only a few degrees of freedom were considered. They consisted in modelling the brake elements as rigid bodies coupled by springs and dampers [5,6]. The main difficulty preventing these models from giving good agreement with reality is the determination of the appropriate spring and damper characteristics. Another class of model is based on the finite element method (FEM). This method is useful to model the different parts of the mechanism in a realistic way.

The different models are also distinguished according to their friction law. In the literature, this ranges from the classical Coulomb friction law with a constant friction coefficient to a velocity-dependent friction coefficient or more complex friction laws.

In this work, the FEM is used to model disc brake squeal of a TGV train (Train à Grande Vitesse) in order to compare the numerical result with experimental squeal frequencies. With this spatial discretization method, the contact conditions are well modelled, so for the sake of simplicity, a local Coulomb friction law is used with a constant friction coefficient. This kind of study has not previously been conducted on TGV trains.

*Corresponding author. Tel.: +33 1 53 42 71 72; fax: +33 1 53 42 97 84.
E-mail addresses: lorang@lms.polytechnique.fr (X. Lorang), florence.margiocchi@sncf.fr (F. Foy-Margiocchi).

0022-460X/$ - see front matter © 2006 Elsevier Ltd. All rights reserved.
doi:10.1016/j.jsv.2005.12.006

2. Introduction

The brake squeal generated by TGV disc brakes is a source of discomfort for the passengers both inside and outside the train. It is therefore important to develop a refined mechanical modelling of the phenomenon in order to understand the mechanism of the squeal generation. The squeal phenomenon is due principally to a self-excited vibration of the brake components, at high frequency (from 4 to 20 kHz), and high intensity (up to 130 dB). It occurs only at low speeds, thus principally when the train arrives at a station. A theoretical and numerical discussion is given here and compared with experimental data in order to understand the principal mechanisms of squeal generation. The TGV disc brake system is first described briefly. Some experimental data are then given obtained at a station from sound pressure measurements taken by microphones close to the discs. Vibration measurements are also presented taken on the brake components of a train at rest. A numerical simulation by the FEM is undertaken and the steady sliding solution is computed. A stability analysis is then performed in order to analyse the flutter instability of the steady sliding response of the pads on the discs, under the assumption of Coulomb friction with a constant friction coefficient.

3. The brake system

The disc-brake system of a TGV train is mounted on a bogie as shown in Fig. 1. There are four discs on each axle. Each disc brake is composed of two symmetric lining plates with cylindrical pads (Fig. 2) which press against the disc. The compression force is about 19 kN at maximum. The discs are attached to the axle by means of a bell which is a very thin structure clamped to the axle, see Fig. 3.

4. Experimental data

The experimental measurements at the station are used to obtain the spectrum of brake squeal. For this, a microphone was mounted near a disc brake as shown in Fig. 4. The spectrum obtained is shown in Fig. 5. This shows clearly the existence of seven frequencies which emerge from the background noise. They occur in the frequency range 6–20 kHz.

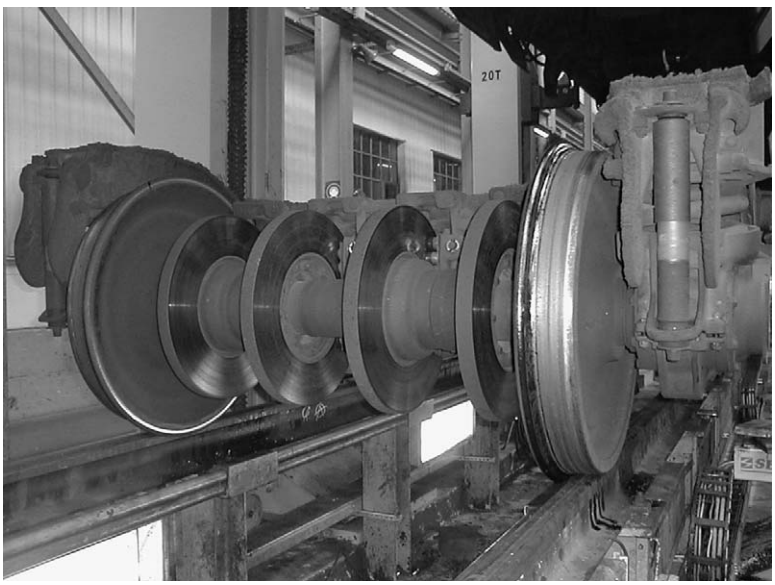

Fig. 1. A TGV bogie showing a wheelset with four brake discs.

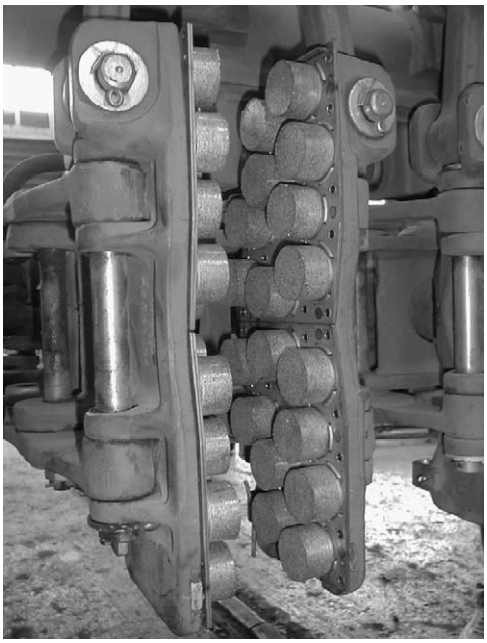

Fig. 2. Brake linings.

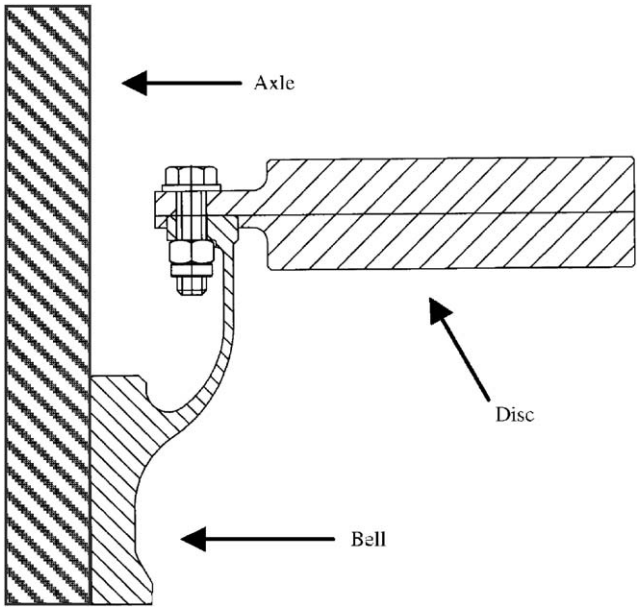

Fig. 3. Sketch of brake disc mounting arrangement.

An experimental modal analysis to determine the modal vibration has been also performed for a bogie at rest. Fig. 6 shows the two frequency response functions superposed with the sound pressure spectrum which shows clearly that some vibration frequencies of the disc coincide also with some measured noise frequencies. The first frequency response function comes from excited bending modes (the transducer measures axial accelerations) whereas the second one is related to in-plane modes.

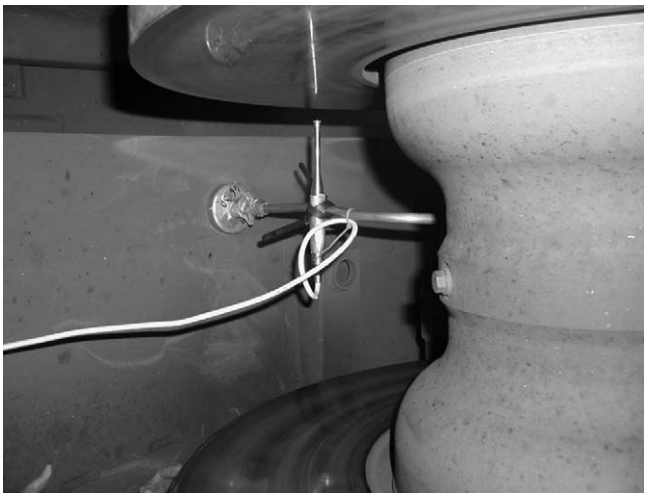

Fig. 4. View of microphone mounted between two brake discs.

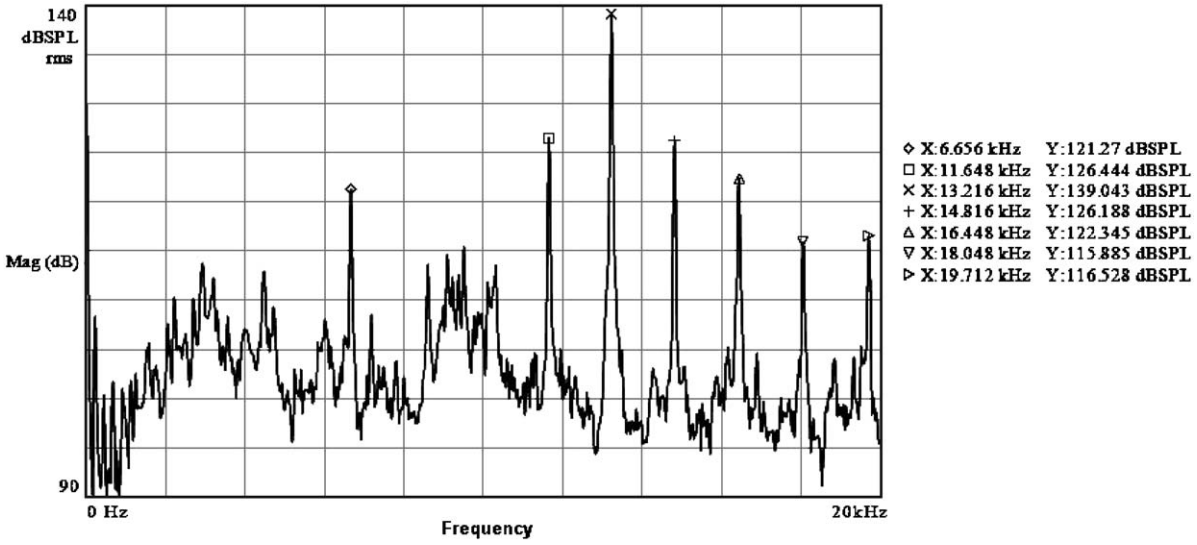

Fig. 5. A typical brake squeal sound pressure spectrum.

5. Mechanical model

The disc and the linings are assumed to be linearly elastic, isotropic and homogeneous solids undergoing small deformation. The contact is unilateral with Coulomb friction and the friction coefficient is assumed constant. A discretization by finite elements (Fig. 7) is adopted with common nodes in contact.

The first model considered was a clamped disc. Different studies have shown that the bell does not add much stiffness to the disc which behaves like a free–free disc. From a numerical point of view it has been found to be necessary to use quadratic elements for the disc and linings to approximate the bending modes correctly. As a consequence, the model is composed of shell elements for the bell and quadratic volume elements for the disc and linings. Table 1 gives a comparison between the natural frequencies of the bell/disc system obtained numerically and the experimental ones.

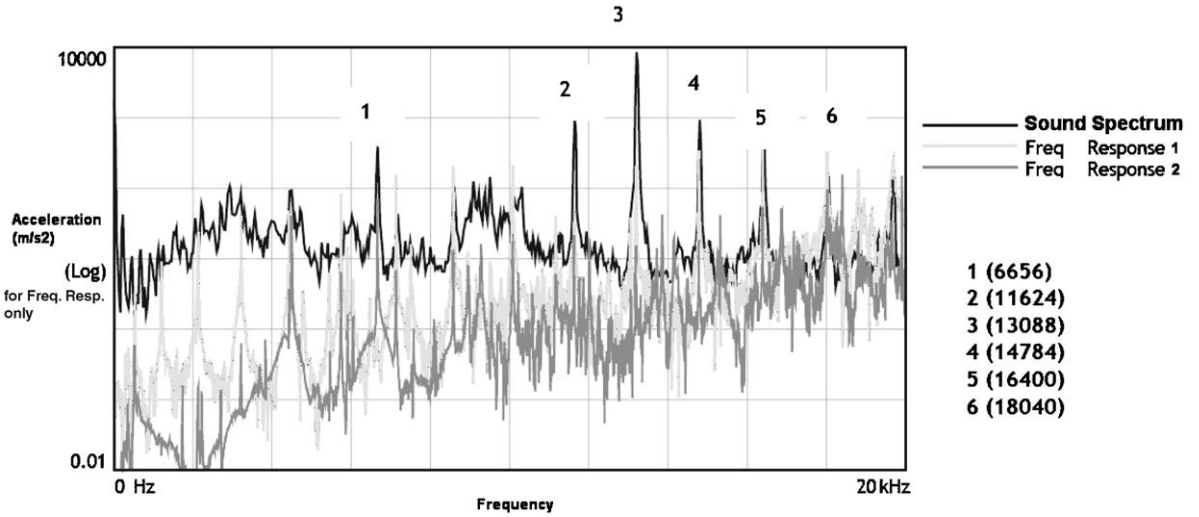

Fig. 6. Two frequency response functions of the brake disc superposed with the sound pressure spectrum from Fig. 5. Light grey: axial acceleration; dark grey: in-plane acceleration; black: sound pressure.

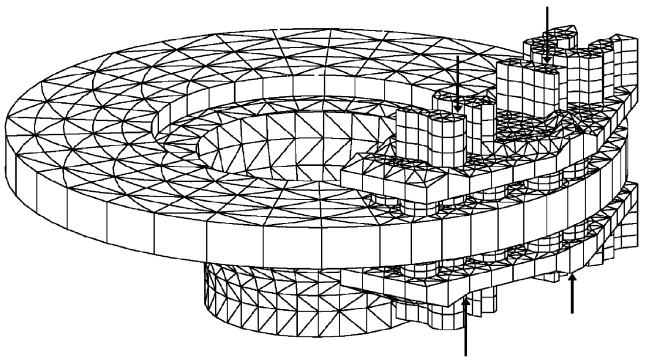

Fig. 7. The finite element model of the brake disc and linings.

Table 1
Comparison of numerical and experimental natural frequencies

Modes with nodal diameters	Finite element model (frequencies Hz)	Experimental results (frequencies Hz)	Relative difference (%)
2	563	520	8.3
3	1206	1200	0.5
4	2101	2120	−0.9
5	3176	3208	−1.0
6	4384	4424	−0.9
7	5697	5736	−0.7
8	7091	7128	−0.5
9	8554	8575	−0.2
10	10 074	10 080	−0.1
11	11 640	11 624	0.1
12	13 232	13 088	1.1
13	14 885	14 784	0.7
14	16 556	16 400	1.0
15	18 254	18 040	1.2

6. The governing equations

The system is governed by the virtual work equation with unilateral and frictional contact conditions. If $\mathbf{u}$ denotes the displacement of the bell/disc D, and $\mathbf{u^L}$ the displacement of the pads/linings L, then:

$$\int_D \boldsymbol{\sigma}(\mathbf{u}) : \boldsymbol{\varepsilon}(\mathbf{u}^*)\,\mathrm{d}\Omega + \int_D \rho.\boldsymbol{\gamma}\cdot\mathbf{u}^*\,\mathrm{d}\Omega = \int_{\partial\Omega_C} N.u_n^* + \mathbf{T}\cdot\mathbf{u}_\mathbf{t}^*\,\mathrm{d}\Omega \quad \forall \mathbf{u}^* \in U_{\mathrm{ad}_0}$$
$$\text{with } U_{\mathrm{ad}_0} = \{\mathbf{u}/\mathbf{u} = 0 \text{ on } \partial\Omega_U\},\ \mathbf{u} = \mathbf{U_g} \text{ on } \partial\Omega_U \tag{1}$$

$$\begin{cases} u_n = \mathbf{u}\cdot\mathbf{n} \\ \mathbf{u_t} = \mathbf{u} - u_n.\mathbf{n} \end{cases} \quad \text{and} \quad \begin{cases} N = (\boldsymbol{\sigma}\cdot\mathbf{n})\cdot\mathbf{n}, \\ \mathbf{T} = \boldsymbol{\sigma}\cdot\mathbf{n} - N.\mathbf{n}, \end{cases}$$

where $\boldsymbol{\sigma}$ is the Cauchy stress tensor, $\boldsymbol{\varepsilon}$ is the strain tensor, $\boldsymbol{\gamma}$ is the acceleration vector, ρ is the density and $\mathbf{U_g}$ is the given displacement vector.

The constitutive equations are:

$$\boldsymbol{\sigma}(\mathbf{u}) = \mathbf{E} : \boldsymbol{\varepsilon}(\mathbf{u}) \quad \text{in } D$$

$$\begin{cases} N \leqslant 0 \\ \mathbf{u}\cdot\mathbf{n} + \mathbf{u^L}\cdot\mathbf{n^L} \leqslant 0 \\ N.[\mathbf{u}\cdot\mathbf{n} + \mathbf{u^L}\cdot\mathbf{n^L}] = 0 \end{cases} \quad \text{and} \quad \begin{cases} |\mathbf{T}| \leqslant -f.N \\ \mathbf{T}\cdot\mathbf{w} - f.N|\mathbf{w}| = 0 \end{cases} \quad \text{on } \partial\Omega_C,$$

where $\mathbf{E}$ is the Hooke fourth-order tensor, $\mathbf{n}$ is the outward normal to the planar surface of the disc and $\mathbf{n^L}$ is the normal to the pads. On the contact surface $\partial\Omega_C$, $\mathbf{n} = -\mathbf{n^L}$.

$\mathbf{w}$ is the sliding velocity, $\mathbf{w} = \mathbf{v} + \dot{\mathbf{u}} - \dot{\mathbf{u}}^\mathbf{L}$, and $\mathbf{v}$ is the velocity due to the rotation of the disc. The coefficient of friction is f.

In a same way, $\mathbf{u^L}$ must satisfy:

$$\int_L \boldsymbol{\sigma}^\mathbf{L}(\mathbf{u^L}) : \boldsymbol{\varepsilon}(\mathbf{u}^*)\,\mathrm{d}\Omega + \int_L \rho^\mathbf{L}.\boldsymbol{\gamma}^\mathbf{L}\cdot\mathbf{u}^*\,\mathrm{d}\Omega = \int_{\partial\Omega_F^L} \mathbf{F}_g\cdot\mathbf{u}^*\,\mathrm{d}\Omega + \int_{\partial\Omega_C} N.u_n^* + \mathbf{T^L}\cdot\mathbf{u}_\mathbf{t}^*\,\mathrm{d}\Omega$$
$$\forall \mathbf{u}^* \in U^L_{\mathrm{ad}_0} \text{ with } U^L_{\mathrm{ad}_0} = \{\mathbf{u}/\mathbf{u} = 0 \text{ on } \partial\Omega^L_U\},\ \mathbf{u^L} = \mathbf{U^L_g} \text{ on } \partial\Omega^L_U,$$

$$\boldsymbol{\sigma}^\mathbf{L}(\mathbf{u^L}) = \mathbf{E^L} : \boldsymbol{\varepsilon}(\mathbf{u^L}) \quad \text{in } L,$$

$$\begin{cases} N \leqslant 0 \\ \mathbf{u}\cdot\mathbf{n} + \mathbf{u^L}\cdot\mathbf{n^L} \leqslant 0 \\ N.[\mathbf{u}\cdot\mathbf{n} + \mathbf{u^L}\cdot\mathbf{n^L}] = 0 \end{cases} \quad \text{and} \quad \begin{cases} |\mathbf{T^L}| \leqslant -f.N \\ \mathbf{T^L}\cdot\mathbf{w^L} - f.N|\mathbf{w^L}| = 0 \end{cases} \quad \text{on } \partial\Omega_C,$$

with $\mathbf{w^L} = -\mathbf{w}$ and $\mathbf{F}_g$ which is the given force on the linings (on $\partial\Omega^L_F$).

Under the assumption of small speed of rotation, the approximation $\boldsymbol{\gamma} = \mathbf{u}_{,tt}$ holds, refer to Ref. [7] for a more complete expression of $\boldsymbol{\gamma}$.

7. The steady sliding response

At the steady sliding equilibrium, $\mathbf{w} = \mathbf{v}$ and $\boldsymbol{\gamma} = \mathbf{0}$. The displacement at equilibrium $\mathbf{u}$ must satisfy from Eq. (1):

$$\int_D \boldsymbol{\varepsilon}(\mathbf{u}) : \mathbf{E} : \boldsymbol{\varepsilon}(\mathbf{u}^*)\,\mathrm{d}\Omega = \int_{\partial\Omega_C} N.u_n^* + \mathbf{T}\cdot\mathbf{u}_\mathbf{t}^*\,\mathrm{d}\Omega \quad \forall \mathbf{u}^* \in U_{\mathrm{ad}_0}$$
$$\text{with } U_{\mathrm{ad}_0} = \{\mathbf{u}/\mathbf{u} = \mathbf{0} \text{ on } \partial\Omega_U\},\ \mathbf{u} = \mathbf{U_d} \text{ on } \partial\Omega_U, \tag{2}$$

with

$$\begin{cases} N \leqslant \mathbf{0} \\ \mathbf{u}\cdot\mathbf{n} + \mathbf{u}^{\mathbf{L}}\cdot\mathbf{n}^{\mathbf{L}} \leqslant \mathbf{0} \\ N.[\mathbf{u}\cdot\mathbf{n} + \mathbf{u}^{\mathbf{L}}\cdot\mathbf{n}^{\mathbf{L}}] = \mathbf{0} \end{cases} \quad \text{and} \quad \mathbf{T} = f.N.\frac{\mathbf{v}}{|\mathbf{v}|} = f.N.\mathbf{t} \quad \text{on } \partial\Omega_C.$$

Similar equations are also satisfied by $\mathbf{u}^{\mathbf{L}}$. The discretized equations are

$$\mathbf{K}.\mathbf{U} = \mathbf{P}, \quad \mathbf{K}^{\mathbf{L}}.\mathbf{U}^{\mathbf{L}} = \mathbf{P}^{\mathbf{L}},$$

respectively, for the disc and the linings.

With the notation $\mathbf{U} = [\mathbf{Y}, \mathbf{U_C}]^{\mathbf{T}}$, where $\mathbf{Y}$ represents the degree of freedom associated with the nodes located outside the contact zone, the force vector $\mathbf{P}$ is

$$\mathbf{P} = \begin{bmatrix} \mathbf{F} \\ \mathbf{R_C} \end{bmatrix}.$$

If $(\mathbf{R_C})_I$ is the (3×1) contact reaction vector at a node I, then the contact conditions for $(\mathbf{U}, \mathbf{U}^{\mathbf{L}})$ and $(\mathbf{R_C}, \mathbf{R}^{\mathbf{L}}_{\mathbf{C}})$ on this node I are:

$$\begin{cases} N_I \leqslant 0 \\ (\mathbf{U_C})_I.\mathbf{n}_I + (\mathbf{U}^{\mathbf{L}}_{\mathbf{C}})_I.\mathbf{n}^{\mathbf{L}}_I \leqslant 0 \\ N_I.[(\mathbf{U_C})_I.\mathbf{n}_I + (\mathbf{U}^{\mathbf{L}}_{\mathbf{C}})_I.\mathbf{n}^{\mathbf{L}}_I] = 0 \end{cases} \quad \text{and} \quad (\mathbf{R_C})_I = N_I(\mathbf{n}_I + f.\mathbf{t}_I).$$

These conditions must be verified for all contact nodes I.

A theoretical discussion can be found in Ref. [7] giving a description of the equilibrium under the form of a linear complementary problem and sufficient conditions for the existence and uniqueness of the steady sliding equilibrium. The computation algorithm to obtain the steady sliding equilibrium (Fig. 8) consists of successive iterations on the contact zone in order to satisfy the contact conditions. Practically, convergence is obtained quickly.

Fig. 9 shows the normal contact force $\mathbf{N}^{\mathbf{e}}$ at equilibrium. It is clear from this figure, that for this given coefficient of friction, f and for this given force on the linings, $\mathbf{F}_g$, the contact zone at equilibrium here is simply the largest possible contact zone ($\partial\Omega^e_C = \partial\Omega_C$).

In the next part, $\mathbf{u_e}$ is the equilibrium displacement and $\partial\Omega^e_C$ the contact zone at equilibrium.

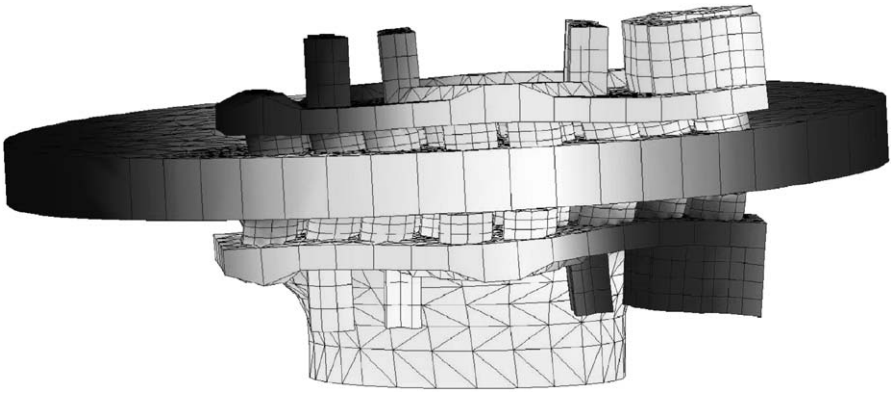

Fig. 8. The sliding equilibrium of the brake system.

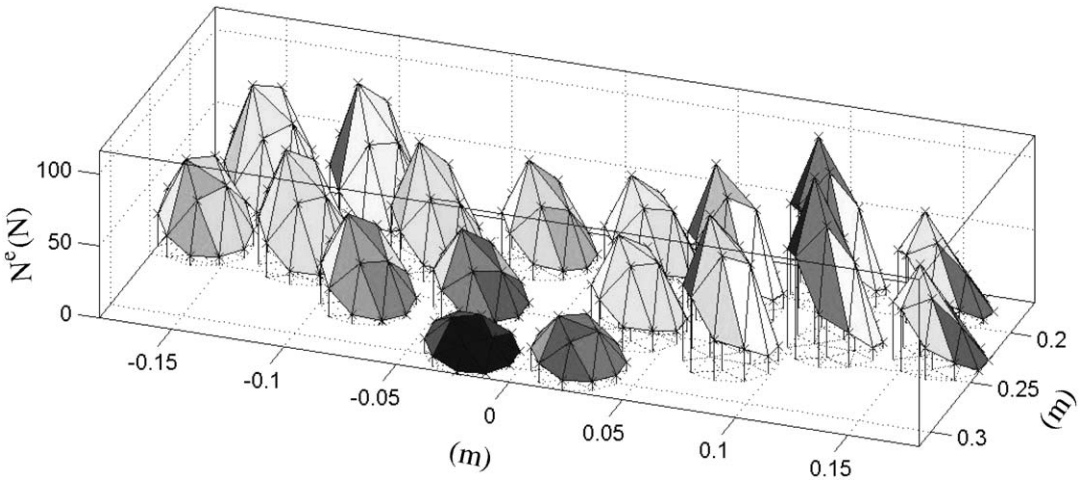

Fig. 9. The local normal contact force N^e (Newton) over $\partial\Omega_C$.

8. The flutter instability of the steady sliding equilibrium

A small perturbed motion near the equilibrium is now considered. However, the governing equations are not differentiable when there is separation, and thus only sliding motions are considered on the present contact zone. Such a perturbed motion $\hat{\mathbf{u}}$ can then be governed by linearized equations. From the expressions:

$$\mathbf{u} = \mathbf{u_e} + \hat{\mathbf{u}}, \quad \hat{\mathbf{u}} \cdot \mathbf{n} + \hat{\mathbf{u}}^{\mathbf{L}} \cdot \mathbf{n}^{\mathbf{L}} = \mathbf{0} \quad \text{on } \partial\Omega_C^e.$$

The contact conditions:

$$\mathbf{T} = f.N.\frac{\mathbf{w}}{|\mathbf{w}|}$$

give, after linearization

$$\hat{\mathbf{T}} = f.\hat{N}.\frac{\mathbf{v}}{|\mathbf{v}|} + \frac{f.N_e}{|\mathbf{v}|}\left(\hat{\mathbf{w}} - \frac{\mathbf{v}\cdot\hat{\mathbf{w}}}{|\mathbf{v}|^2}\mathbf{v}\right) = f.\hat{N}.\mathbf{t} + \frac{f.N_e}{|\mathbf{v}|}(\mathbf{1} - \mathbf{t}\otimes\mathbf{t}).\hat{\mathbf{w}}, \tag{3}$$

with $\hat{\mathbf{w}} = \hat{\mathbf{u}}_{,\mathbf{t}} - \hat{\mathbf{u}}^{\mathbf{L}}_{,\mathbf{t}} = (\mathbf{1} - \mathbf{n}\otimes\mathbf{n})(\hat{\mathbf{u}}_{,\mathbf{t}} - \hat{\mathbf{u}}^{\mathbf{L}}_{,\mathbf{t}})$ under the condition $\hat{\mathbf{u}}\cdot\mathbf{n} + \hat{\mathbf{u}}^{\mathbf{L}}\cdot\mathbf{n}^{\mathbf{L}} = \mathbf{0}$ ($\otimes$ is the tensor product: $\mathbf{n}\otimes\mathbf{n}$ is the second-order tensor $n_m n_n$).

The second term of $\hat{\mathbf{T}}$ is due to the planar nature of the friction force.

The perturbed displacement $\hat{\mathbf{u}}$ is thus governed by

$$\int_D \rho.\hat{\mathbf{u}}_{,\mathbf{tt}}\cdot\mathbf{u}^*\,\mathrm{d}\Omega + \int_D \boldsymbol{\varepsilon}(\hat{\mathbf{u}}) : \mathbf{E} : \boldsymbol{\varepsilon}(\mathbf{u}^*)\,\mathrm{d}\Omega = \int_{\partial\Omega_C} \hat{N}.u_n^* + \hat{\mathbf{T}}\cdot\mathbf{u}_\mathbf{t}^*\,\mathrm{d}\Omega \tag{4}$$

or by

$$\int_D \rho.\hat{\mathbf{u}}_{,\mathbf{tt}}\cdot\mathbf{u}^*\,\mathrm{d}\Omega - \int_{\partial\Omega_C^e}\frac{f.N_e}{|\mathbf{v}|}[(\mathbf{1}-\mathbf{t}\otimes\mathbf{t}).\hat{\mathbf{w}}]\cdot\mathbf{u}^*\,\mathrm{d}\Omega + \int_D \boldsymbol{\varepsilon}(\hat{\mathbf{u}}) : \mathbf{E} : \boldsymbol{\varepsilon}(\mathbf{u}^*)\,\mathrm{d}\Omega$$
$$= \int_{\partial\Omega_C^e} \hat{N}.u_n^* + f.\hat{N}.\mathbf{t}\cdot\mathbf{u}_\mathbf{t}^*\,\mathrm{d}\Omega.$$

For the sake of clarity, the term

$$-\int_{\partial\Omega_C^e}\frac{f.N_e}{|\mathbf{v}|}[(\mathbf{1}-\mathbf{t}\otimes\mathbf{t}).\hat{\mathbf{w}}]\cdot\mathbf{u}^*\,\mathrm{d}\Omega$$

is first neglected.

Under this assumption (A), the discretized dynamic equations are the following. If $\mathbf{U}$ is the column vector associated with the discretization of $\hat{\mathbf{u}}$ and $\mathbf{N}$ is associated with $\hat{N}$, then the discretization of Eq. (4) under assumption (A) gives

$$\begin{gathered}\mathbf{M}.\ddot{\mathbf{U}}+\mathbf{K}.\mathbf{U}=\mathbf{P}=\begin{bmatrix}\mathbf{0}\\ \mathbf{R_C}\end{bmatrix},\quad \mathbf{M^L}.\ddot{\mathbf{U}}^{\mathbf{L}}+\mathbf{K^L}.\mathbf{U^L}=-\mathbf{P},\\ (\mathbf{U_C})_I.\mathbf{n}_I+(\mathbf{U_C^L})_I.\mathbf{n}_I^{\mathbf{L}}=\mathbf{0}\quad \forall I.\end{gathered}\tag{5}$$

For the system of D and L bodies, Eq. (5) can be written as

$$\begin{gathered}\begin{bmatrix}\mathbf{M} & \mathbf{0}\\ \mathbf{0} & \mathbf{M^L}\end{bmatrix}.\ddot{\mathbf{U}}^{\mathbf{TOT}}+\begin{bmatrix}\mathbf{K} & \mathbf{0}\\ \mathbf{0} & \mathbf{K^L}\end{bmatrix}.\mathbf{U^{TOT}}=\begin{bmatrix}\mathbf{P}\\ -\mathbf{P}\end{bmatrix},\\ (\mathbf{U_C})_I.\mathbf{n}_I+(\mathbf{U_C^L})_I.\mathbf{n}_I^{\mathbf{L}}=\mathbf{0},\quad \forall I\Rightarrow \mathbf{A}^{\mathrm{T}}.\mathbf{U^{TOT}}=\mathbf{0},\end{gathered}\tag{6}$$

with $\mathbf{U^{TOT}}=[\mathbf{U},\mathbf{U^L}]^{\mathrm{T}}$.

From Eq. (6), for the node I, and for D, it follows that:

$$(\mathbf{M})_I\ddot{\mathbf{U}}+(\mathbf{K})_I\mathbf{U}=N_I(\mathbf{n}_I+f.\mathbf{t}_I),\tag{7}$$

we can then calculate $N_I=\mathbf{n}_I^{\mathrm{T}}(\mathbf{M})_I\ddot{\mathbf{U}}+\mathbf{n}_I^{\mathrm{T}}(\mathbf{K})_I\mathbf{U}$, $(\mathbf{M})_I$ and $(\mathbf{K})_I$ are $(3\times N_{\mathrm{dof}})$ matrices (N_{dof} is the number of degrees of freedom of D). Then, we have

$$f.N_I.\mathbf{t}_I=f.[(\mathbf{t}_I\otimes\mathbf{n}_I)(\mathbf{M})_I]\ddot{\mathbf{U}}+f.[(\mathbf{t}_I\otimes\mathbf{n}_I)(\mathbf{K})_I]\mathbf{U}.$$

Eq. (7) then gives $[(\mathbf{M})_I-f(\mathbf{M_f})_I]\ddot{\mathbf{U}}+[(\mathbf{K})_I-f(\mathbf{K_f})_I]\mathbf{U}=N_I\mathbf{n}_I$.

It is then possible to build $\tilde{\mathbf{M}}$ and $\tilde{\mathbf{K}}$ as follows:

$$\tilde{\mathbf{M}}.\ddot{\mathbf{U}}+\tilde{\mathbf{K}}.\mathbf{U}=\begin{bmatrix}\mathbf{0}\\ \tilde{\mathbf{R}}_{\mathbf{C}}\end{bmatrix},\quad (\tilde{\mathbf{R}}_{\mathbf{C}})_I=N_I\mathbf{n}_I,$$

where $\tilde{\mathbf{M}}$ and $\tilde{\mathbf{K}}$ are *non-symmetric* matrices.

$$\tilde{\mathbf{K}}=\mathbf{K}-f.\mathbf{K_f}\quad\text{and}\quad\tilde{\mathbf{M}}=\mathbf{M}-f.\mathbf{M_f}.$$

Doing the same thing for L, it is possible to write Eq. (6) as follows:

$$\begin{gathered}\begin{bmatrix}\tilde{\mathbf{M}} & \mathbf{0}\\ \mathbf{0} & \tilde{\mathbf{M}}^{\mathbf{L}}\end{bmatrix}.\ddot{\mathbf{U}}^{\mathbf{TOT}}+\begin{bmatrix}\tilde{\mathbf{K}} & \mathbf{0}\\ \mathbf{0} & \tilde{\mathbf{K}}^{\mathbf{L}}\end{bmatrix}.\mathbf{U^{TOT}}=\begin{matrix}[\mathbf{0} & \tilde{\mathbf{R}}_{\mathbf{C}}]^{\mathrm{T}}\\ [\mathbf{0} & \tilde{\mathbf{R}}_{\mathbf{C}}^{\mathbf{L}}]^{\mathrm{T}}\end{matrix}=-\mathbf{A}.\mathbf{N},\\ \mathbf{A}^{\mathrm{T}}.\mathbf{U^{TOT}}=\mathbf{0},\end{gathered}$$

so that the global dynamic system is obtained:

$$\begin{bmatrix}\mathbf{M^{TOT}}(f) & \mathbf{0}\\ \mathbf{0} & \mathbf{0}\end{bmatrix}\begin{bmatrix}\ddot{\mathbf{U}}^{\mathbf{TOT}}\\ \ddot{\mathbf{N}}\end{bmatrix}+\begin{bmatrix}\mathbf{K^{TOT}}(f) & \mathbf{A}\\ \mathbf{A}^{\mathrm{T}} & 0\end{bmatrix}.\begin{bmatrix}\mathbf{U^{TOT}}\\ \mathbf{N}\end{bmatrix}=\begin{bmatrix}\mathbf{0}\\ \mathbf{0}\end{bmatrix}.$$

Now, consider what happens without the assumption A:

$(\mathbf{R_C})_I$ can be written as follows:

$$(\mathbf{R_C})_I=N_I(\mathbf{n}_I+f.\mathbf{t}_I)+\frac{f.N_{eI}}{|\mathbf{v}_I|}[(\mathbf{1}-\mathbf{t}_I\otimes\mathbf{t}_I)(\mathbf{1}-\mathbf{n}_I\otimes\mathbf{n}_I)((\dot{\mathbf{U}}_{\mathbf{C}})_I-(\mathbf{U_C^L})_I)].$$

Taking into account $(\mathbf{R}_{\mathbf{C}}^{\mathbf{L}})_I$, the additional term leads to the following element damping matrix:

$$\mathbf{C}_I^{\text{elem}}(f)\cdot\begin{bmatrix}(\dot{\mathbf{U}}_{\mathbf{C}})_I\\(\dot{\mathbf{U}}_{\mathbf{C}}^{\mathbf{L}})_I\end{bmatrix} = -\frac{f.N_{eI}}{|\mathbf{v}_I|}\begin{bmatrix}(\mathbf{1}+\mathbf{t}_I\otimes\mathbf{t}_I)(\mathbf{1}-\mathbf{n}_I\otimes\mathbf{n}_I) & -(\mathbf{1}-\mathbf{t}_I\otimes\mathbf{t}_I)(\mathbf{1}-\mathbf{n}_I\otimes\mathbf{n}_I)\\ -(\mathbf{1}-\mathbf{t}_I\otimes\mathbf{t}_I)(\mathbf{1}-\mathbf{n}_I\otimes\mathbf{n}_I) & (\mathbf{1}-\mathbf{t}_I\otimes\mathbf{t}_I)(\mathbf{1}-\mathbf{n}_I\otimes\mathbf{n}_I)\end{bmatrix}\cdot\begin{bmatrix}(\dot{\mathbf{U}}_{\mathbf{C}})_I\\(\dot{\mathbf{U}}_{\mathbf{C}}^{\mathbf{L}})_I\end{bmatrix}.$$

Then, the global dynamic problem can be written as

$$\begin{bmatrix}\mathbf{M}^{\mathbf{TOT}}(f) & \mathbf{0}\\ \mathbf{0} & \mathbf{0}\end{bmatrix}\begin{bmatrix}\ddot{\mathbf{U}}^{\mathbf{TOT}}\\ \ddot{\mathbf{N}}\end{bmatrix}+\begin{bmatrix}\mathbf{C}^{\mathbf{TOT}}(f) & \mathbf{0}\\ \mathbf{0} & \mathbf{0}\end{bmatrix}\begin{bmatrix}\dot{\mathbf{U}}^{\mathbf{TOT}}\\ \dot{\mathbf{N}}\end{bmatrix}+\begin{bmatrix}\mathbf{K}^{\mathbf{TOT}}(f) & \mathbf{A}\\ \mathbf{A}^{\mathrm{T}} & \mathbf{0}\end{bmatrix}.\begin{bmatrix}\mathbf{U}^{\mathbf{TOT}}\\ \mathbf{N}\end{bmatrix}=\begin{bmatrix}\mathbf{0}\\ \mathbf{0}\end{bmatrix}. \tag{8}$$

The aim of this method is to find the modal form of Eq. (8). However, since the dimension of the matrices considered is very large, it is necessary to restrict the displacement in an appropriate basis composed of the first free vibration modes of the associated system with contact but without friction. In this basis, the mass and stiffness and damping matrices are the projected matrices of small dimension.

The basis Φ composed of the free vibration modes is defined as follows:

$$\left(\lambda^2\begin{bmatrix}\mathbf{M}^{\mathbf{TOT}}(0) & \mathbf{0}\\ \mathbf{0} & \mathbf{0}\end{bmatrix}+\begin{bmatrix}\mathbf{K}^{\mathbf{TOT}}(0) & \mathbf{A}\\ \mathbf{A}^{\mathrm{T}} & \mathbf{0}\end{bmatrix}\right).\boldsymbol{\Phi}=\mathbf{0}.$$

If $\boldsymbol{\Phi}=\begin{bmatrix}\boldsymbol{\Phi}_{\mathbf{U}}\\ \boldsymbol{\Phi}_{\mathbf{N}}\end{bmatrix}$, $\begin{bmatrix}\mathbf{U}^{\mathbf{TOT}}\\ \mathbf{N}\end{bmatrix}=\boldsymbol{\Phi}.\mathbf{Z}$ and $\mathbf{Z}=\boldsymbol{\Psi}.e^{\lambda.t}$, the small dimension problem is

$$\left(\lambda^2.\boldsymbol{\Phi}^{\mathrm{T}}\begin{bmatrix}\mathbf{M}^{\mathbf{TOT}}(f) & \mathbf{0}\\ \mathbf{0} & \mathbf{0}\end{bmatrix}\boldsymbol{\Phi}+\lambda.\boldsymbol{\Phi}^{\mathrm{T}}\begin{bmatrix}\mathbf{C}^{\mathbf{TOT}}(f) & \mathbf{0}\\ \mathbf{0} & \mathbf{0}\end{bmatrix}\boldsymbol{\Phi}+\boldsymbol{\Phi}^{\mathrm{T}}\begin{bmatrix}\mathbf{K}^{\mathbf{TOT}}(f) & \mathbf{A}\\ \mathbf{A}^{\mathrm{T}} & \mathbf{0}\end{bmatrix}\boldsymbol{\Phi}\right).\boldsymbol{\Psi}=\begin{bmatrix}\mathbf{0}\\ \mathbf{0}\end{bmatrix}.$$

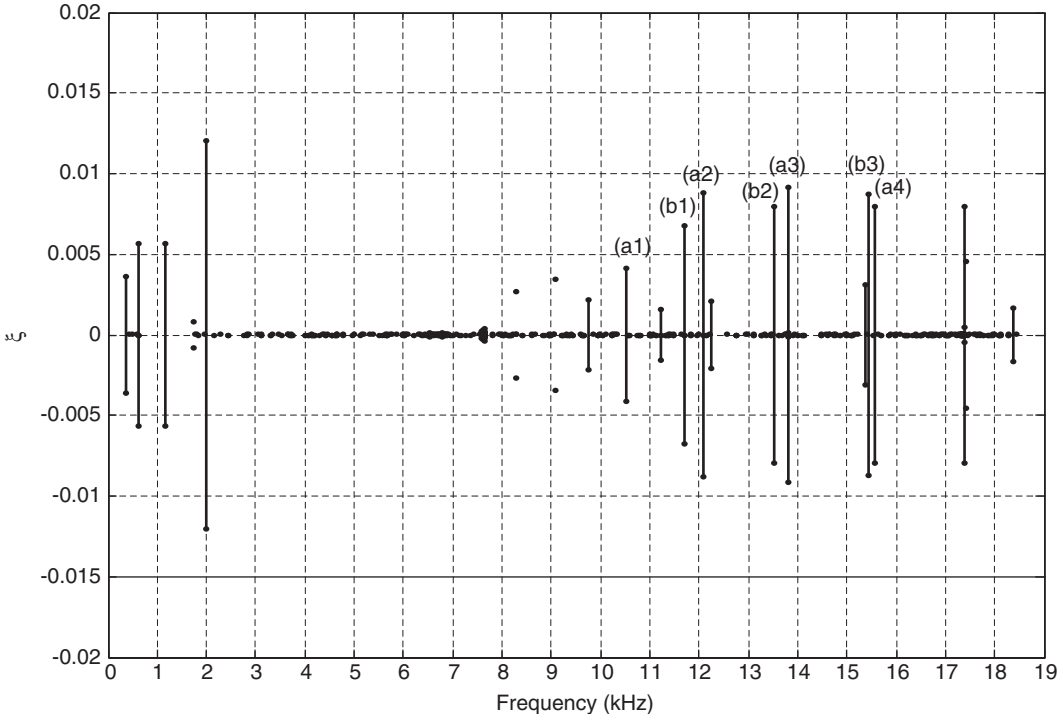

Fig. 10. Eigenvalues in the complex plane without taking account of damping matrix, $\xi=\mathrm{Re}(\lambda)/|\lambda|$ is plotted as a function of the frequency.

The following *generalized eigenvalue problem* is then obtained:

$$\{\lambda^2.\hat{\mathbf{M}} + \lambda.\hat{\mathbf{C}} + \hat{\mathbf{K}}\}.\boldsymbol{\Psi} = \mathbf{0}.$$

The lack of symmetry of these matrices leads to complex modes and to complex eigenvalues. A mode is unstable if $\mathrm{Re}(\lambda)>0$. For an unstable mode, there is flutter instability with a growing displacement in the form:

$$\begin{bmatrix} \mathbf{U}^{\mathbf{TOT}}(t) \\ \mathbf{N}(t) \end{bmatrix} = \mathrm{e}^{\mathrm{Re}(\lambda)t}\boldsymbol{\Phi}.[\mathrm{Re}(\boldsymbol{\Psi})\cos(\mathrm{Im}(\lambda)t) - \mathrm{Im}(\boldsymbol{\Psi})\sin(\mathrm{Im}(\lambda)t)].$$

Figs. 10 and 11 present the results of the eigenvalue analysis. $\xi = \mathrm{Re}(\lambda)/|\lambda|$ is plotted as a function of the frequency ($\mathrm{Im}(\lambda)/2\pi$). In the figures, the straight lines are disc modes whereas the points are lining modes.

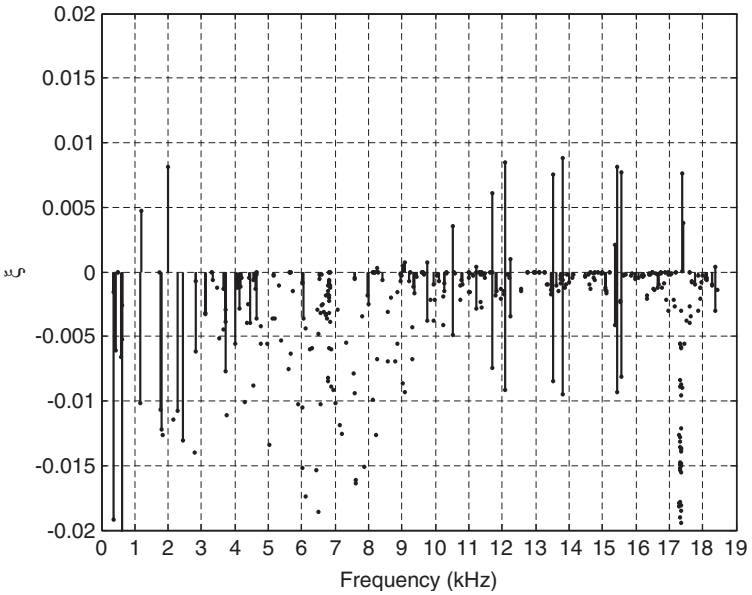

Fig. 11. Eigenvalues in the complex plane with the effect of the damping matrix, $\xi = \mathrm{Re}(\lambda)/|\lambda|$ is plotted as a function of the frequency.

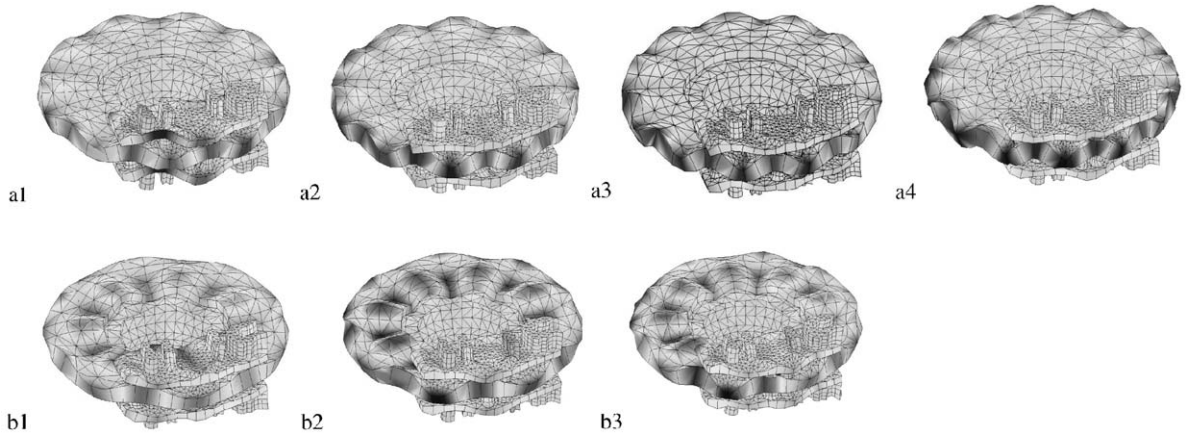

Fig. 12. Unstable modes in braking system.

It is possible to compare ξ with the modal damping ratio of the material. From Figs. 10 and 11, the maximum of ξ can be seen to be about 1%. A modal damping ratio of 1% would then be sufficient to stabilize the modes.

In Fig. 10, the results are presented without taking into account the damping matrix due to the planar effect of friction. Fig. 11 shows that the damping matrix introduced stabilizes all the modes although it is clear that the unstable modes between 10 and 20 kHz are not so much modified.

Fig. 12 shows the main unstable modes of the brake system as identified in Fig. 10. According to the experimental results, it is clear that there is a good agreement between the modes (a1–a4) and reality. From Fig. 12a, modes can be recognized with 10, 11, 12 and 13 nodal diameters, as listed in Table 1. However, the frequencies of the modes (b1–b3) seem to be absent from the noise spectrum. These modes are nodal diameters modes with one nodal circle.

9. Conclusion and future work

This paper presents some interesting directions of research to understand the mechanism of brake squeal. The numerical analysis gives the flutter modes. For some modes, there is a good agreement between the numerical analysis and the experiments. However, the phenomenon is not yet completely explained.

This is the first step of the analysis. Future work to be considered consists of computing the cyclic response resulting from this dynamic bifurcation in the sense of Hopf [8].

References

[1] N.M. Kinkaid, O.M. O'reilly, P. Papadopoulos, Automotive disc brake squeal, *Journal of Sound and Vibration* 267 (2003) 105–166.
[2] D.A. Crolla, A.M. Lang, Brake noise and vibration: state of art, *Vehicle Tribology* 18 (1991) 165–174.
[3] F. Moirot, Etude de la Stabilité d'un Équilibre en Présence du Frottement de Coulomb. Application au Crissement des Freins à Disque. Thèse, Ecole Polytechnique, Paris, 1998.
[4] J.A.C. Martins, J. Guimaraes, L.O. Faria, Dynamic surface solutions in linear elasticity and viscoelasticity with frictional boundary conditions, *Journal of Vibration and Acoustics* 117 (1995) 445–451.
[5] H. Murakami, N. Tsunada, T. Kitamura, A study concerned with a mechanism of disc brake squeal, Technical Report 841233, SAE, Warrendale, PA, 1984.
[6] M.R. North, Disc brake squeal, in: *Braking of Road Vehicles*, *Automobile Division of the Institution of Mechanical Engineers*, Mechanical Engineering Publications Limited, London, England, 1976, pp. 169–176.
[7] F. Moirot, Q.S. Nguyen, Brake squeal: a problem of flutter instability of the steady sliding solution?, *Archives of Mechanics* 52 (2000) 645–662.
[8] F. Moirot, Q.S. Nguyen, An example of stick-slip waves, *Comptes Rendus Mécanique* 328 (2000) 663–669.